Journal of Materials Science: Materials in Electronics (2019) 30:19513–19523
https://doi.org/10.1007/s10854-019-02317-6

Barium deficiency and sintering temperature effects on structural and transport properties of $La_{0.5}Eu_{0.2}Ba_{0.3-x}\square_xMnO_3$ manganites

Amira khlifi[1] · A. Mleiki[1,2] · H. Rahmouni[1] · N. Guermazi[3] · K. Khirouni[4] · A. Cheikhrouhou[2]

Received: 13 May 2019 / Accepted: 9 October 2019 / Published online: 14 October 2019

Abstract

$La_{0.5}Eu_{0.2}Ba_{0.3-x}\square_xMnO_3$ ($x=0.00$, 0.05 and 0.15) samples were prepared using sol–gel method and annealed at $T_s=750$ and 950 °C. The X-ray diffraction technique shows that all samples crystallize in the rhombohedral structure with *R*-3c space group. Electrical properties of the prepared compounds were investigated using impedance spectroscopy technique in a wide temperature range (80–440 K). The results show a semiconductor behavior for all samples. From dc-conductivity (σ_{dc}) analysis, it is observed that increasing barium-deficiency content and sintering temperature improves the electrical conductivity. It is also found that the conduction mechanism is governed by hopping process. Ba-deficiency and sintering temperature affects the activation energy (E_a). From σ_{dc}, in the temperature range of 250–480 K and at $T_s=750$ °C, it is found that E_{a1} decreases from 190 meV for $x=0.00$ to 164 meV for $x=0.15$. Also, for $x=0.00$, E_{a1} decreases from 165 meV at $T_s=750$ °C to 145 meV at $T_s=950$ °C. Complex impedance analysis indicates the presence of non-Debye type relaxation. Such analysis confirms the contribution of grain boundary on the conduction. The activation energy E_{a2} deduced from dc-conductivity matches very well with the value estimated from relaxation time ($E_{a\tau}$) indicating that relaxation and transport mechanisms are related to the same defect.

1 Introduction

From more than 50 years, complex oxides of transition metals have been the immense interest due to their simple structure and interesting physical properties. Notable examples are manganite having the colossal magnetoresistance [1] and multiferroic oxides such as hexaferrite based barium [2–4]. In the mixed valence manganite with general formula $La_{1-x}A_xMnO_3$, where A is a divalent element (A = Ca, Ba, Sr…), several research groups are interested due to the strong interplay between structural, magnetic and electrical properties as well as the possibility of technologic application [5–7]. These materials exhibit a very rich phase diagram due to the subtle competition among the interactions involving spin, lattice and charge degree of freedom [8]. Due to their physical properties, manganite are used as cathode material in solid oxide fuel SOFC [9, 10], computer memory system, infrared detectors, magnetic cooling system, recording devices and photocatalysis [11–16]. It is well known that lanthanum manganite $LaMnO_3$ have an insulator behavior. Such compound display both ferromagnetic state and metallic conductivity when trivalent La^{3+} ions are partially substituted by divalent ions as Ca^{2+}, Ba^{2+} and Sr^{2+} [17–19]. These substitutions cause the creation of mixed valence of manganese ions giving rise to double-exchange (DE) interaction which explains successfully the metallic behavior. Moreover, the existing of Jahn–Teller distortion plays a significant role in determining the magneto-transport properties [20]. In addition, a change in magnetic states of oxides, e.g., ferromagnetic or antiferromagnetic behavior, was resulting from the modification in the element dopant, the preparation methods or the cation deficiency. For example, the La–Ba manganite exhibit a long range ferromagnetic

✉ A. Mleiki
alimlk1986@hotmail.com

1 Unité de Recherche Matériaux Avancés et Nanotechnologies (URMAN), Institut Supérieur des Sciences Appliquées et de Technologie de Kasserine, Kairouan University, BP 471, 1200 Kasserine, Tunisia

2 LT2S, Digital Research Center of Sfax, Sfax Technoparc, 3021 Sfax, Tunisia

3 Laboratoire Génie des Matériaux et Environnement (LGME), Ecole Nationale d'Ingénieurs de Sfax (ENIS), Université de Sfax, Sfax, Tunisia

4 Laboratoire de Physique des Matériaux et des Nanomatériaux Appliquée à l'Environnement, Faculté des Sciences de Gabès cité Erriadh, Université de Gabès, 6079 Gabès, Tunisia

interaction and large magnetoresistance above room temperature [21]. As regards, $La_{0.65}Ba_{0.35}MnO_3$ system has $T_C = 362$ K. Turkanov et al. [22] have been reported that the $La_{1-x}Ba_xMnO_{3-x/2}$ samples are semiconductors and show considerable magnetoresistance over a wide temperature range in a magnetically ordered state. In addition, the electrical properties of these samples depends to the barium content. Indeed, the $La_{1-x}Ba_xMnO_3$ ($0.25 \le x \le 0.35$) system exhibit an increase remarkably of semiconductor to metal transition temperature (T_{SM}) from $T_{SM} = 200$ K for $x = 0.25$ to 230 K for $x = 0.35$ [23]. In literature [24, 25], structural, electrical, magnetic and magnetocaloric properties of $La_{0.7-x}Eu_xBa_{0.3}MnO_3$ system have been investigated. The properties of such compounds depend on Eu content. It is found that the sample with $x = 0.15$ is a good candidate as a magnetic refrigerant. The replacing of La^{3+} ions by smaller Eu^{3+} ions ($r(La^{3+}) = 1.216$ Å $> r(Eu^{3+}) = 1.120$ Å for a 9 coordination [26]) affects the crystalline network, reduce the DE interactions and then introduce the decrease of electrical conductivity. Also, the physical properties of ceramics are sensitive to the sintering temperature [27–33]. In fact, the results confirmed that the magnetic, electronic and transport properties are significantly affected by the grain size. Among these reports, the decrease of sintering temperature (T_s) into $La_{1-x}Ce_xMnO_3$ ($x = 0.3$, 0.4 and 0.5) [30] provokes the change of the structure from the orthorhombic to the rhombohedral system which induces an increase of the magnetization. In addition, the effect of sintering temperature (T_s), from 600 to 1000 °C, in $Pr_{0.5}Eu_{0.1}Sr_{0.4}MnO_3$ [31] exhibit that the sample sintered at 1000 °C displays superior magnetic properties. It is reported that such result is due to the largest crystallite and grain size. Also, Venkataiah et al. [32] and Baaziz et al. [33] have investigated the effect of T_s on electrical properties of $La_{0.67}Ca_{0.33}MnO_3$ and $La_{0.67}Sr_{0.33}MnO_3$ respectively and demonstrated that the increase of T_s induces the increase of particle size. Such works confirm that the annealing temperature promotes the growth of grain and improve the quality of crystalline materials. In addition, many authors display that the presence of vacancies in perovskite manganites improves their physical properties [34, 35]. A-site deficiencies in this system provoke the variation of the ratio of Mn^{3+}/Mn^{4+}. Oumezzine et al. [36] show that the barium vacancies in $La_{0.67}Ba_{0.33-x}\square_xMnO_3$ ($x = 0.00$, 0.05 and 0.1) manganite modify the structural parameters and a decrease of T_{SM} has been observed. Nevertheless, the discussion of the effect of deficiencies and sintering temperature in manganite systems are not intensively studied.

In the present work, we investigate the effect of barium deficiency and sintering temperature on the structural and electrical properties of $La_{0.5}Eu_{0.2}Ba_{0.3-x}\square_xMnO_3$ compounds. Such compounds are synthesized by Pechini sol–gel with $x = 0.00$, 0.05 and 0.15 and sintered at $T_s = 750$ and 950 °C.

2 Experimental details

Nano-polycrystalline powders of $La_{0.5}Eu_{0.2}Ba_{0.3-x}\square_xMnO_3$ with $x = 0.00$, 0.05 and 0.15 were prepared using sol–gel method [37]. In this process, stoichiometric amounts of the nitrate $La(NO_3)_3{\cdot}6H_2O$, Ba $(NO_3)_2$, $Eu(NO_3)_3$ and $Mn(NO_3)_2{\cdot}6H_2O$ were dissolved in distilled water. Citric acid and ethylene glycol were added in the solution. A stable solution was formed. Then, the solution was stirred and heated at 80 °C to eliminate the excess water and obtain a viscous gel. The gel was ground for 1 h and calcined at 600 °C for 6 h. Different packages of powder were pressed into pellets and were sintered at 750 and 950 °C for 4 h. Finally, to avoid the lack of oxygen stoichiometry the obtained pellet is quenched rapidly in air at room temperature. Consequently, the oxygen stoichiometry for our samples has been considered ideal [38, 39]. The phase purity and crystallinity of the powder were examined by the X-ray diffractometer ["Panalytical X pert Pro" diffractometer with Cu-Kα radiation ($\lambda = 1.5406$ Å)]. Also, we used the Scherrer's formula to estimate, from the X-ray (104) diffraction peak, the average particle size for all investigated samples. To obtain electrical measurements, and for allow from the surface of the electrode precise calculations, a thin silver film on both pellet side was deposited through a circular mask with a diameter of 6 mm. Therefore, a configuration of a plate capacitor was obtained to measure both the conductance and the capacitance. In order to vary the temperature from 80 to 480 K, the samples were mounted in a cryostat. The measurements were conducted under vacuum and in the dark using an Agilent 4294 analyzer with a signal amplitude of 50 mV.

3 Results and discussions

3.1 X-ray diffraction analysis

The crystal structure of the $La_{0.5}Eu_{0.2}Ba_{0.3-x}\square_xMnO_3$ ($x = 0.00$, 0.05 and 0.15) samples, prepared at different sintering temperatures (750 and 950 °C), has been analyzed by X-ray diffraction (XRD). The XRD patterns as well as the Miller index are shown in Fig. 1a–f. The result shows a single phase and no impurities are detected which indicates high purity of the samples. As can be seen in Fig. 1a–c, at 750 °C sintering temperature, single-phase $La_{0.5}Eu_{0.2}Ba_{0.3-x}\square_xMnO_3$ powders show a broad distribution due to the nanocrystalline character. It can also be seen that most of the peaks are relatively high, which reveals that the samples crystallized perfectly.

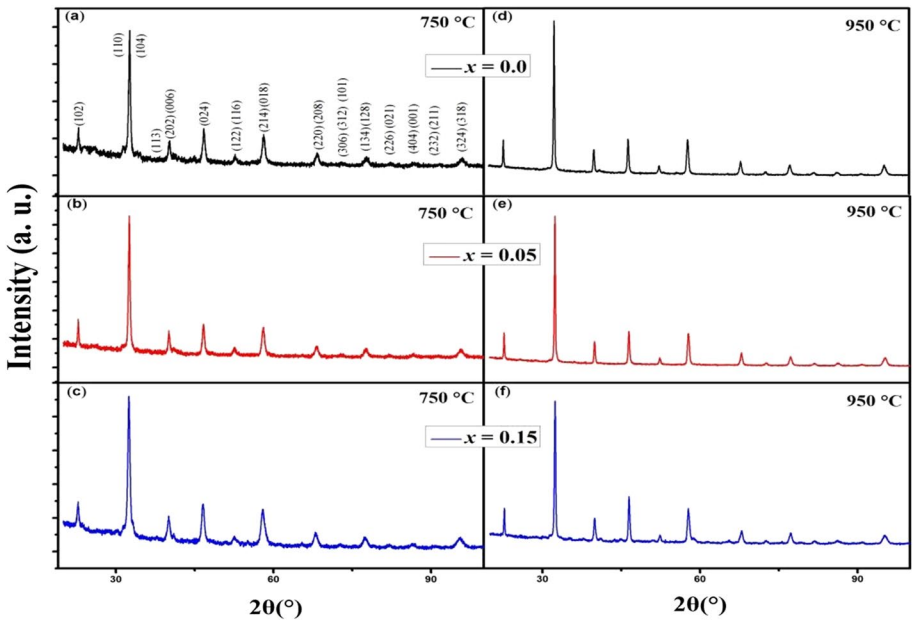

Fig. 1 X-ray diffraction patterns of $La_{0.5}Eu_{0.2}Ba_{0.3-x}\square_xMnO_3$ ($x=0.00$, 0.05 and 0.15) samples annealed at 750 °C (**a**–**c**) and at 950 °C (**d**–**f**)

Furthermore, all the diffraction peaks in both the series are assigned well to rhombohedral crystalline phase with the R-3c space group. For the same sample, the degree of crystallinity is observed to increase as the reaction temperature is increased from 750 to 950 °C since the corresponding XRD peaks became more intense and narrower. In order to obtain the crystallite size, the Scherrer equation was used and the results are listed in Table 1.

3.2 Conductivity analysis

3.2.1 Dc-conductivity

Figure 2a and b displays the variation of dc-conductivity (σ_{dc}), for $La_{0.5}Eu_{0.2}Ba_{0.3-x}\square_xMnO_3$ ($x=0.00$, 0.05 and 0.15) compounds annealed at 750 and 950 °C. All samples show a semiconductor behavior. In the whole explored temperature range, the metal–semiconductor transition is not observed for all barium vacancies. It has been observed that σ_{dc} values increase with increasing barium deficiency. This result can be related to the rise of the interaction between Mn^{3+} and Mn^{4+} spins which disfavors the charge localization. Moreover, it is clearly shown that the increase of sintering temperature (T_s) from 750 to 950 °C induced an increase of conductivity. This evolution was attributed to the increase of particle size as observed in Table 1. For example, for $x=0.00$, the particle size increases from 26 nm at $T_s=750$ °C to 39 nm at $T_s=950$ °C. This leads to a decrease in the number of grain boundaries which causes a decrease of the scattering of the charge carriers [36]. The reduction of the encountered barriers leads to the enhancement of electrical conductivity.

In order to get information about the conduction mechanism present in the system, experimental data are fitted using various models. In the first hand, the experimental data are well fitted by Mott and Davis law [40].

$$\sigma T = \sigma_0 \exp\left(\frac{E_a}{k_B T}\right), \tag{1}$$

where σ_0 is a pre-exponential factor, E_a is the activation energy and k_B is the Boltzmann constant. The plots of (σT) versus 1000/T shown in Fig. 2c and d are linear over a wide temperature range (250–480 K), confirming a thermally activated polaron hopping. In the other hand, at low temperature, the experimental data are well fitted by another function [40].

$$\sigma = A \exp\left(\frac{-T_0}{T}\right)^{1/4}, \tag{2}$$

where T_0 and A are constant. At low temperature, Fig. 2e and f show a linear evolution of (σ) versus ($1/T^{1/4}$),

Table 1 Crystallite size of $La_{0.5}Eu_{0.2}Ba_{0.3-x}\square_xMnO_3$ ($x=0.00$, 0.05, and 0.15) samples annealed at 750 and 950 °C

Sintering temperature (°C)	750			950		
Samples	$x=0.00$	$x=0.05$	$x=0.15$	$x=0.00$	$x=0.05$	$x=0.15$
Crystallite size (nm)	26	25	19	39	41	37

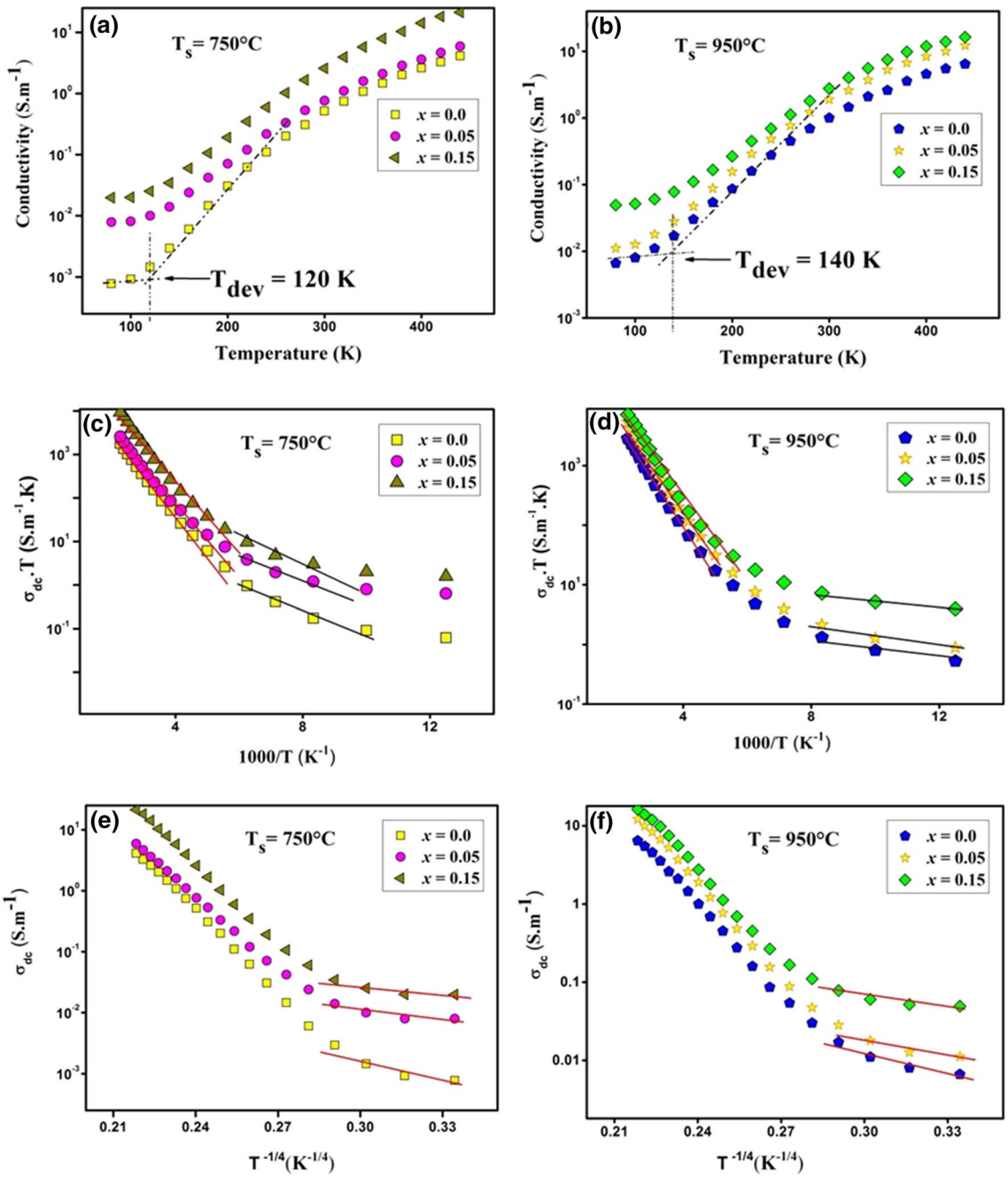

Fig. 2 **a**, **b** Temperature dependence of dc-conductivity of $La_{0.5}Eu_{0.2}Ba_{0.3-x}\square_xMnO_3$ manganites, sintered at different temperatures (750 and 950 °C). **c**, **d** Variation of (σT) versus (1000/T). **e**, **f** Variation of (σ) versus ($T^{-1/4}$)

suggesting that the conduction mechanism is dominated by variable range hopping (VRH). From the linear part of Fig. 2c and d, in the temperature range of 250–480 K, we deduce the activation energy (E_{a1}) value. The variation of activation energy as a function of barium vacancy, at different sintering temperatures, is shown in Fig. 3. It is found that E_{a1} depends strongly in Ba-vacancy. It decreases from 190 meV for $x = 0.00$ to 164 meV for $x = 0.15$ at $T_s = 750$ °C and from 165 meV for $x = 0.00$ to 145 meV for $x = 0.15$ at $T_s = 950$ °C. The increase of Ba-vacancy concentration induces the increase of the number of Mn^{3+}/Mn^{4+} pair ions and the change of internal chemical factors, which leads to a decrease of E_{a1} as observed in Table 2. Furthermore, the increase of sintering temperature leads to an important decrease of E_{a1} value. The interaction between grains increases with the increase in particle size. Such evolution

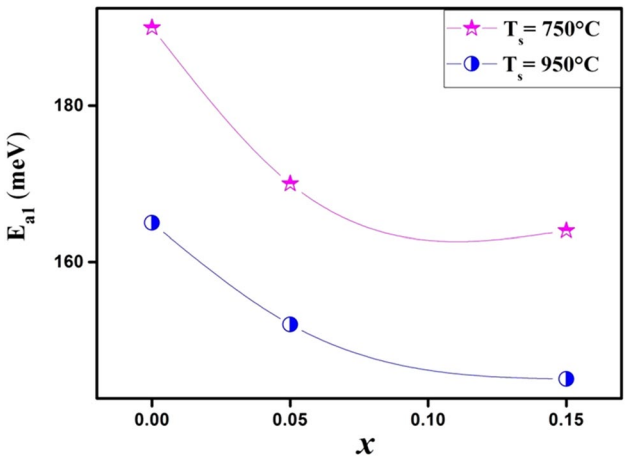

Fig. 3 Variation of the activation energy (E_{a1}) as a function barium-vacancy concentration and sintering temperature

Table 2 Activation energy values inferred from the temperature dependence of relaxation time and conductivity

T_s (°C)	x	E_{a1} (meV) (250–480 K)	E_{a2} (meV) (100–250 K)	$E_{a\tau}$ (meV) (100–250 K)
750	0.0	190	88	83
	0.05	170	52	49
	0.15	164	44	39
950	0.0	165	11	11
	0.05	152	15	13
	0.15	145	21	20

reinforced the possibility of conduction electron to hop to the neighboring sites [35], therefore the value of E_{a1} decreases.

3.2.2 Ac-conductivity analysis

It is well known that ac measurements give quite relevant information about properties such as conductivity, loss factor and capacitance [41]. Figure 4a–f shows the variation of ac-conductivity as a function of temperature and frequency for the investigated compounds, sintered at different temperatures. The obtained result can be separated into three regions. In the first region (R-I) it is observed that conductivity increases slightly with both frequency and temperature. According to Jacob et al. [42], the increase of conductivity with temperature can be attributed to the thermally enhanced drift mobility of charge carriers. In the second region (R-II) and in the specific temperature range (ΔT), it is clear that the conductivity, for all samples, becomes almost frequency independent. In such a range, we suggest that the capacitor character is reduced. According to the summarized results in Table 1 and for $T_s = 950$ °C, it is noticed that ΔT and crystallite size vary in the same manner when increasing barium vacancy. When the crystallite size decreases, the density of grain boundary rises leading to the increase of capacitor character. Such an explanation is confirmed by the variation of ΔT and crystallite size of the compound sintered at $T_s = 950$ °C. When the temperature increases, the frequency dependence of conductivity becomes less significant. Therefore, the frequency independent portion dominates [43]. In addition, the change of sintering temperature from 750 to 950 °C leads to a decrease of ΔT range for all samples. In the third region (R-III), the conductivity decreases with increasing frequency. For $f = 3 \times 10^6$ Hz, a semiconductor–metal transition temperature was detected for all investigated samples. The presence of metallic behavior can be related to the DE interaction between Mn^{3+} and Mn^{4+} ions [44]. For $T_s = 750$ °C, the value of transition temperature (T_{SM}) does not change ($T_{SM} = 300$ K) when the barium vacancy increase from $x = 0.05$ to $x = 0.15$. It is further noticed from Fig. 4a–f that the increase of sintering temperature shifts the values of T_{SM} to a lower temperature region. Li et al. [44] explain the decrease of transition temperature with increasing sintering temperature by the increase of oxygen vacancies.

3.3 Complex impedance analysis

Figure 5a–f shows the variation of reel part of impedance (Z′) with frequency, at different temperatures, of $La_{0.5}Eu_{0.2}Ba_{0.3-x}\square_xMnO_3$ system with $x = 0.00$, 0.05 and 0.15. The spectra are characterized by the decrease of Z′ with an increase in temperatures and frequencies. Such evolution confirms the observed increase in ac-conductivity with temperature and frequency [45]. At higher frequencies, the merge of the impedance (Z′) at each temperature indicates the presence of space charge. Such behavior can be attributed to the lowering of the barriers properties in the materials which reduce the resistive behavior with the rise in temperature [46]. From Z′ spectrum, we can calculate the Average Normalized Change (ANC) [47]. Such a parameter is considered as the intrinsic response of the sample. It is inferred using the relation $ANC = (\Delta Z'/\Delta f)/Z'_0$, where ΔZ′ is the difference between the value Z'_{low} of Z' at low frequency (f_{low}) and Z'_{high} of Z′ at high frequency (f_{high}). Δf is the difference between f_{low} and f_{high}. The Z'_0 is the Z′ value at zero frequency [45]. The temperature dependence of ANC and dANC/dT for $x = 0.0$ sintered at different temperatures, is shown in Fig. 5g and h. The ANC decreases when the temperature increases. Such behavior indicated the manifestation of different conduction process [43]. The slope of d(ANC)/dT at any temperature reflects the density of the released trapped charges [48, 49]. For $x = 0.00$, the change of the slope occurs at 120 and 140 K for $T_s = 750$ and 950 °C, respectively. The T_{ANC} values are in good agreement with the temperature T_{dev} values observed in σ_{dc} (t) curves when the conductivity begins to increase rapidly. So,

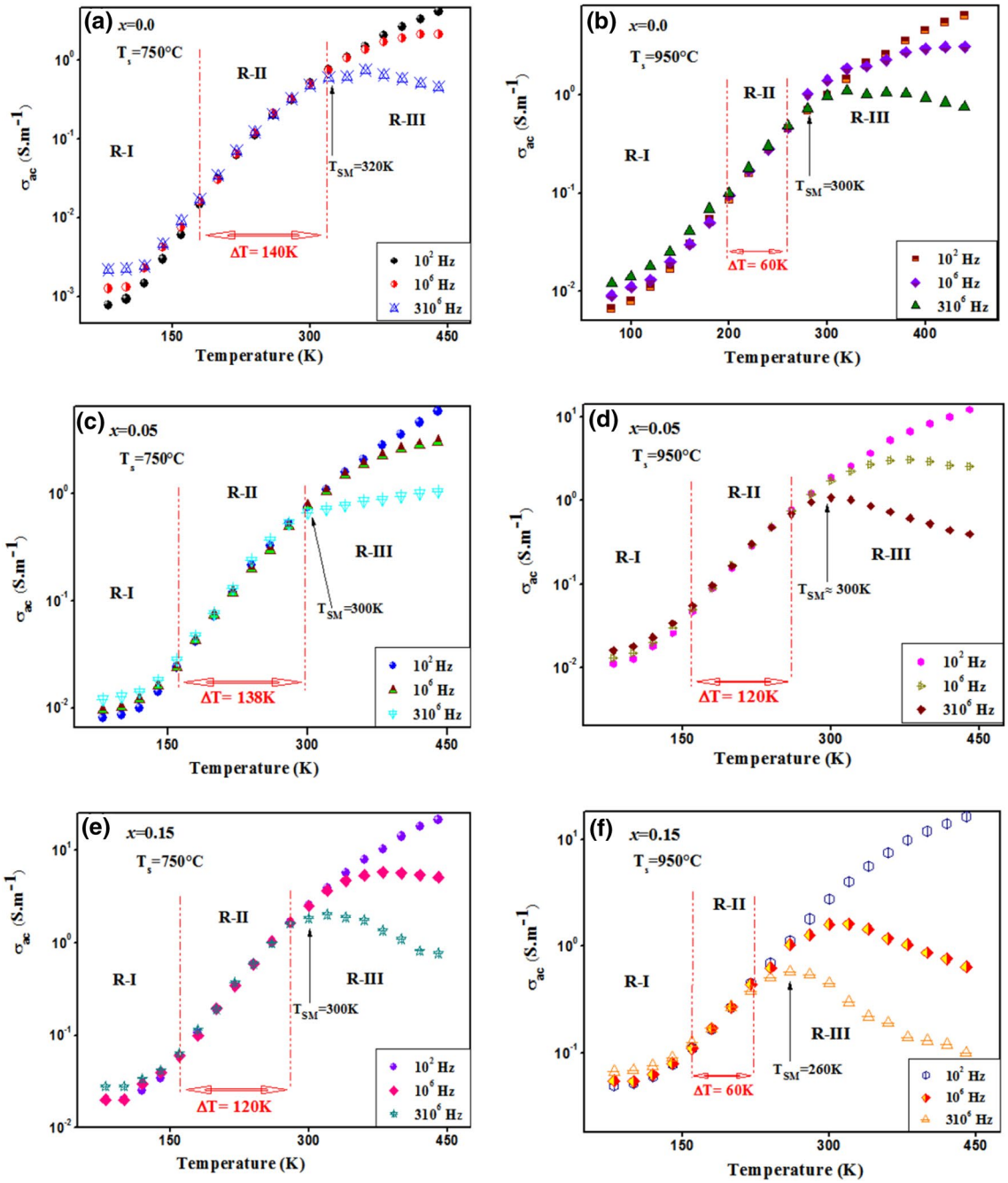

Fig. 4 Variation of (σ_{ac}) as a function of temperature at selected frequencies (10^2 Hz, 10^6 Hz, and 3×10^6 Hz) for $La_{0.5}Eu_{0.2}Ba_{0.3-x}\square_xMnO_3$

the increase in conductivity is related to the released carriers from trapped centers. Additionally, Fig. 6a–f shows the variation of the imaginary part of the impedance (Z″) as a function of frequency at different temperatures. The spectra are characterized by the appearance of a single peak for each temperature at a certain frequency f_r called "relaxation frequency". The relaxation frequency is not the same for all peaks. Such behavior reflects the non-Debye type of relaxation in the system [50]. Also, the height of the relaxation peaks decreases when the temperature increases indicating the drop in the resistive properties [35, 51, 52]. The contribution of the relaxation process may possibly be explained by the presence of electrons/species at lower temperatures and defects/vacancies at high temperatures [53]. In order to calculate the relaxation time at each temperature, we used the relation $2\pi f_r\tau = 1$. For all investigated compounds, the relaxation time is plotted against 1000/T (see Fig. 6g, h). For the temperature range of 100–250 K, the plot of (σT)

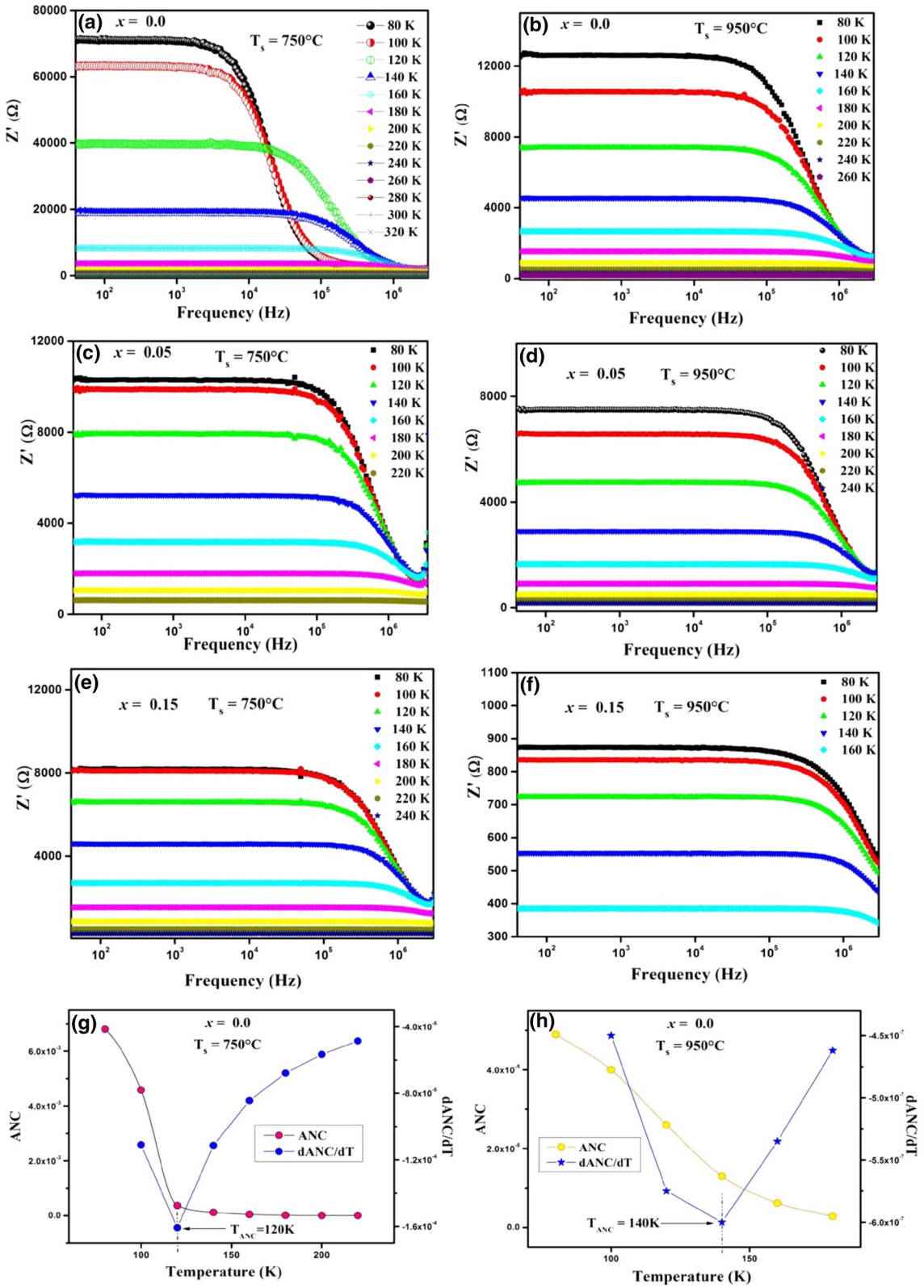

Fig. 5 **a**–**f** Frequency and temperature dependence of the real part of impedance (Z′) of $La_{0.5}Eu_{0.2}Ba_{0.3-x}\square_xMnO_3$. **g**, **h** Temperature dependence of average normalized change (ANC) and dANC/dT for $La_{0.5}Eu_{0.2}Ba_{0.3-x}\square_xMnO_3$ ($x = 0.00$) sintered at different temperatures (750 and 950 °C)

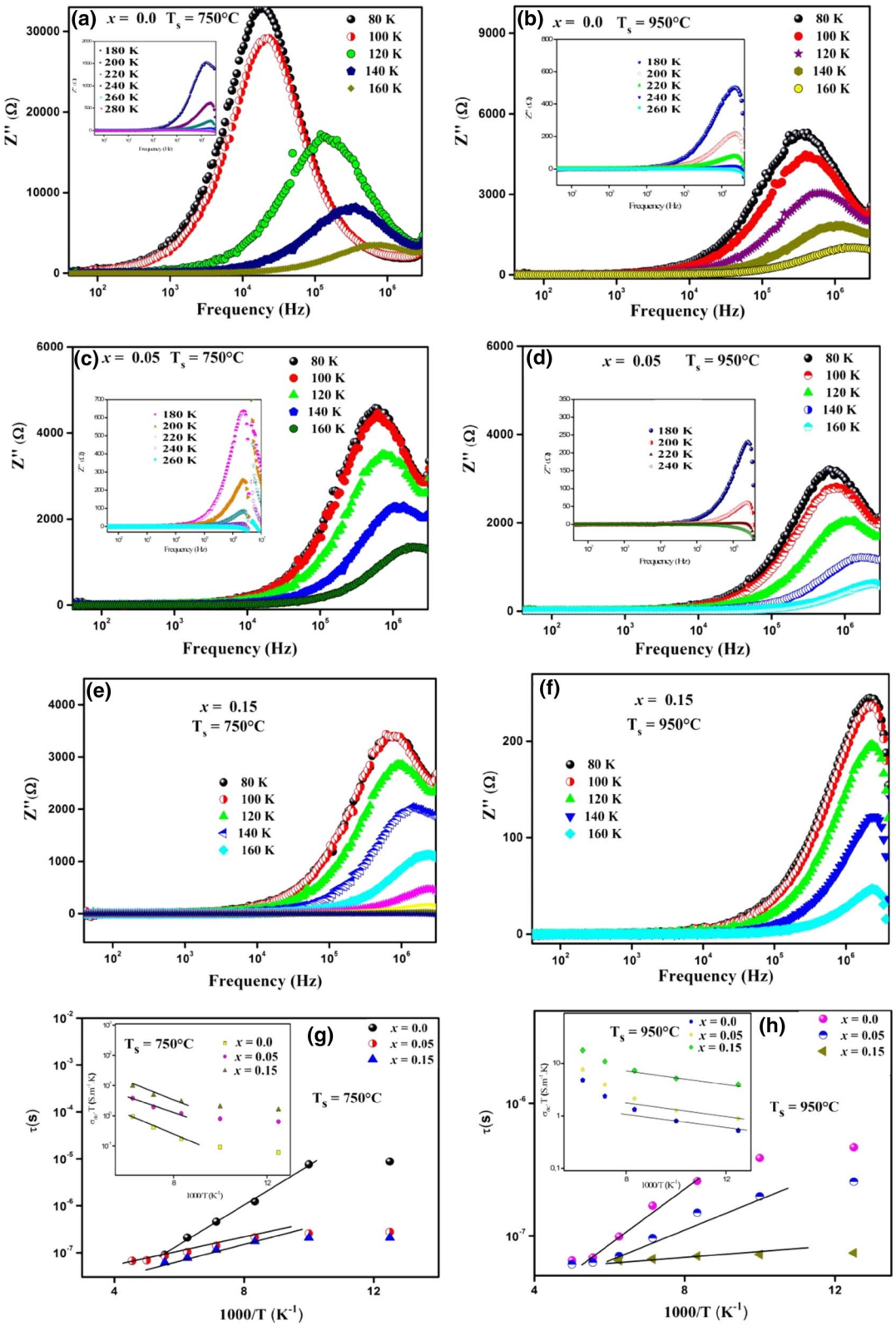

Fig. 6 **a**–**f** Frequency and temperature dependence of the imaginary part of impedance (Z″) for $La_{0.5}Eu_{0.2}Ba_{0.3-x}\square_xMnO_3$. **g**, **h** Plots of relaxation time τ versus 1000/T

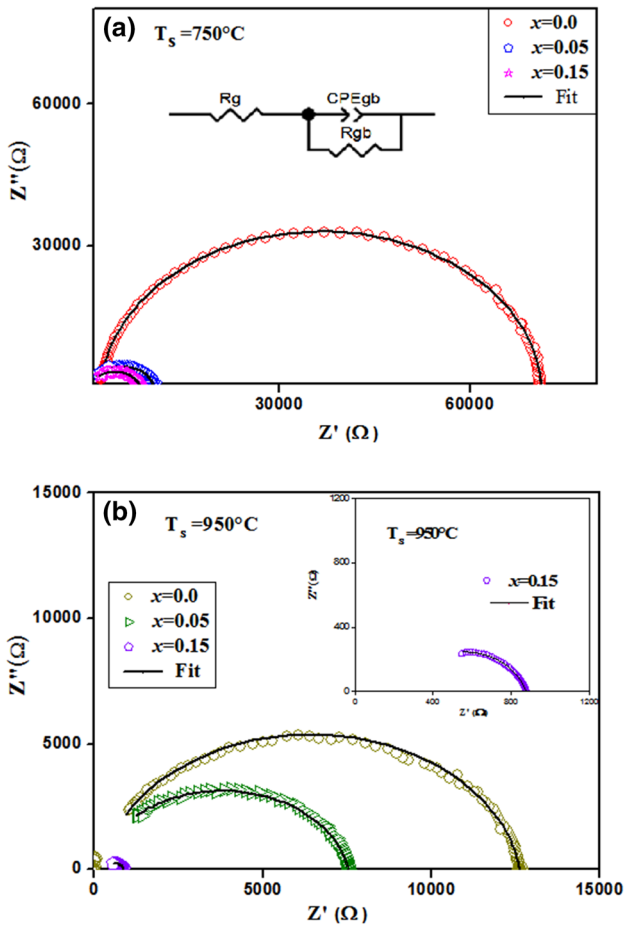

Fig. 7 Nyquist plot at T = 80 K for $La_{0.5}Eu_{0.2}Ba_{0.3-x}\square_xMnO_3$ [sintered at 750 °C (**a**) and at 950 °C (**b**)]. The inset shows the electrical equivalent circuit

versus 1000/T is shown in the inset of Fig. 6g and h. From the slope of the curves, the activation energy values was deduced. The values from both relaxation time ($E_{a\tau}$) and conductivity (E_{a2}) are listed in Table 2. It is clear that these values are equal. So, the relaxation process and electrical conductivity are related to the same defect. Complex impedance plots of $La_{0.5}Eu_{0.2}Ba_{0.3-x}\square_xMnO_3$ system with $x = 0.00$, 0.05 and 0.15 at T = 80 K, for different sintering temperature, are shown in Fig. 7a and b. A single semicircular is observed. Such observation suggests the contribution of intrinsic grain interior (bulk) property of the materials [54, 55]. As the barium-deficiency and sintering temperature increase, the diameters of semi-circular decreases. The observed evolution is in good agreement with the increase of the dc-conductivity and indicates the reduction of grain interior resistance. Also, it is noticed that the complex impedance plots are not represented by a full semicircle. Moreover, their centers are depressed below the real axis (Z′) indicating the non-Debye type of relaxation process [56]. The observed behavior can be related to the presence of the distributed elements in the system [57]. Shamim et al. [58] show that the origin of non-Debye relaxation phenomenon is correlated to the strain–stress phenomenon, orientations defects, grain size, and oxygen vacancies. Zview software was used to fit the obtained curves. The complex impedance is successfully modeled to an electrical equivalent circuit (inset of Fig. 7a): [Rg (resistance of the grains) in series with a circuit (R_{gb}// CPE_{gb})] which describes the response of grains boundaries. The introduced constant phase element (CPE) in the circuit described the non-ideal capacitor behavior which can be related to the presence of more than one relaxation process with the same time relaxation [59].

4 Conclusion

The effect of barium deficiency and sintering temperature on structural and transport properties of $La_{0.5}Eu_{0.2}Ba_{0.3-x}\square_xMnO_3$ ($x = 0.00$, 0.05 and 0.15) are investigated using, respectively, XRD and impedance spectroscopy techniques. XRD studies confirmed that the samples crystallize in the rhombohedral structure with *R*-3c space group. Electrical measurement reveals that all samples exhibit a semiconductor behavior. Further, the conduction mechanism is dominated by thermally activated hopping of small polaron at high temperatures and by variable range hopping at low temperatures. It is found that increasing sintering temperature and barium deficiency enhances electrical conductivity. Also, a non-Debye type relaxation process was noticed and can be correlated to the defects, grain size, and vacancies.

Compliance with ethical standards

Conflicts of interest The authors declare that they have no conflict of interest.

References

1. M. Hennion, S. Petit, A. Ivanov, D. Lamago, J.P. Castellan, Interacting chains of orbital polarons in the colossal magnetoresistance material $La_{1-x}Sr_xMnO_3$ revealed by spin and lattice dynamics. Phys. Rev. B **99**, 214416 (2019)
2. A. Trukhanov, L. Panina, S. Trukhanov, V. Turchenko, M. Salem, Evolution of structure and physical properties in Al-substituted Ba-hexaferrites. Chin. Phys. B **25**, 016102 (2016)
3. S.V. Trukhanov, A.V. Trukhanov, V.A. Turchenko, V.G. Kostishyn, L.V. Panina, I.S. Kazakevich, A.M. Balagurov, Structure and magnetic properties of $BaFe_{11.9}In_{0.1}O_{19}$ hexaferrite in a wide temperature range. J. Alloys. Compd. **689**, 383 (2016)
4. A.V. Trukhanov, V.G. Kostishyn, L.V. Panina, S.H. Jabarov, V.V. Korovushkin, S.V. Trukhanov, E.L. Trukhanova, Magnetic properties and Mössbauer study of gallium doped M-type barium hexaferrites. Ceram. Int. **43**, 12822 (2017)

5. R. von Helmolt, J. Wecker, B. Holzapfel, L. Schultz, K. Samwer, Giant negative magnetoresistance in perovskitelike $La_{2/3}Ba_{1/3}MnO_x$ ferromagnetic films. Phys. Rev. Lett. **71**, 2331 (1993)
6. S. Jin, T.H. Tiefel, M. McCormack, R.A. Fastnacht, R. Ramesh, L.H. Chen, Thousand fold change in resistivity in magnetoresistive La–Ca–Mn–O films. Science **264**, 413 (1994)
7. Y. Tokura, *Colossal Magnetoresistive Oxides* (Gordon and Breach Science, New York, 2000)
8. A. Mleiki, S. Othmani, W. Cheikhrouhou-Koubaa, A. Cheikhrouhou, E.K. Hlil, Normal and inverse magnetocaloric effect and short-range ferromagnetic interaction in $(Pr, Sm)_{0.5}Sr_{0.5}MnO_3$ phase separated manganite. J. Alloys Compd. **688**, 1214 (2016)
9. U.H. Anderson, Review of p-type doped perovskite materials for SOFC and other applications. Solid State. Ion. **52**, 33 (1992)
10. N.Q.J. Minh, Ceramics fuel cells. Am. Ceram. Soc. **76**, 563 (1993)
11. A. Mleiki, S. Othmani, W. Cheikhrouhou-Koubaa, A. Cheikhrouhou, E.K. Hlil, Enhanced relative cooling power in Ga-doped $La_{0.7}(Sr, Ca)_{0.3}MnO_3$ with ferromagnetic-like canted state. RSC Adv. **6**, 53602 (2016)
12. Z.C. Xia, S.L. Yuan, W. Feng, L.J. Zhang, G.H. Zang, J. Tang, L. Liu, D.W. Liu, Q.H. Zheng, L. Chen, Z.H. Fang, S. Liu, C.Q. Tang, Large room temperature magnetoresistance in YSZ doped $La_{0.67}Ba_{0.33}MnO_3$ composite. Solid State Commun. **127**, 572 (2003)
13. N. Khare, D.P. Singh, H.K. Gupta, P.K. Siwach, O.N. Srivastava, Preparation and study of silver added $La_{0.67}Ca_{0.33}MnO_3$ film. J. Phys. Chem. Sol. **65**, 867 (2004)
14. S. Tarhouni, A. Mleiki, I. Chaaba, H.B. Khelifa, W. Cheikhrouhou-Koubaa, M. Koubaa, E.K. Hlil, Structural, magnetic and magnetocaloric properties of Ag-doped $Pr_{0.5}Sr_{0.5-x}Ag_xMnO_3$ manganites ($0.0 \leq x \leq 0.4$). Ceram. Int. **43**, 133 (2017)
15. A. Arabi, M. Fazli, M.H. Ehsani, Tuning the morphology and photocatalytic activity of $La_{0.7}Ca_{0.3}MnO_3$ nanorods via different mineralizer-assisted hydrothermal syntheses. Mater. Res. Bull. **90**, 205 (2017)
16. F. Rahmani Afje, M.H. Ehsani, Size-dependent photocatalytic activity of $La_{0.8}Sr_{0.2}MnO_3$ nanoparticles prepared by hydrothermal synthesis. Mater. Res. Exp. **5**, 045012 (2018)
17. O. Chmaissem, B. Dabrowski, S. Kolesnik, J. Mais, J.D. Jorgensen, S. Short, C.E. Botez, P.W. Stephens, Effects of A-site ordering on the structures and properties of $La_{1-x}Ba_xMnO_3$ ($x \sim 0.5$). Phys. Rev. B **72**, 104426 (2005)
18. K. Dörr, Ferromagnetic manganites: spin-polarized conduction versus competing interactions. J. Phys. D **39**, R125 (2006)
19. E. Dagotto, Complexity in strongly correlated electronic systems. Science **309**, 257 (2005)
20. R. Selmi, W. Cherif, L. Fernández Barquín, M. de la Fuente Rodríguez, L. Ktari, Structure and spin glass behavior in $La_{0.77}Mg_{0.23-x\square x}MnO_3$ ($0 \leq x \leq 0.2$) manganites. J. Alloy Compd. **738**, 528 (2018)
21. S.V. Trukhanov, Magnetic and magnetotransport properties of $La_{1-x}BaxMnO_{3-x/2}$ perovskite manganites. J. Mater. Chem. **13**, 347 (2003)
22. S.V. Trukhanov, L.S. Lobanovski, M.V. Bushinsky, I.O. Troyanchuk, H. Szymczak, Magnetic phase transitions in the anion-deficient $La_{1-x}Ba_xMnO_{3-x/2}$ ($0 \leq x \leq 0.50$) manganites. J. Phys. **15**, 1783 (2003)
23. I. Mansuri, D. Varshney, Structure and electrical resistivity of $La_{1-x}Ba_xMnO_3$ ($0.25 \leq x \leq 0.35$) perovskites. J. Alloys. Compd. **513**, 256 (2012)
24. J. Dhahri, A. Dhahri, E. Dhahri, Structural, magnetic and magnetocaloric properties of $La_{0.7-x}Eu_xBa_{0.3}MnO_3$ perovskites. J. Magn. Magn. Mat. **321**, 4128 (2009)
25. H. Rahmouni, B. Cherif, R. Jemai, A. Dhahri, K. Khirouni, Europium substitution for lanthanium in LaBaMnO: the structural and electrical properties of $La_{0.7-x}Eu_xBa_{0.3}MnO_3$ perovskite. J. Alloy Compd. **690**, 890 (2017)
26. R.D. Shannon, Revised effective ionic radii and systematic studies of interatomic distances in halides and chalcogenides. Acta Crystallogr. A **32**, 751 (1976)
27. C.-X. Li, B. Yang, S.-T. Zhang, R. Zhang, W.-W. Cao, Effects of sintering temperature and poling conditions on the electrical properties of $Ba_{0.70}Ca_{0.30}TiO_3$ diphasic piezoelectric ceramics. Ceram. Int. **39**, 2967 (2013)
28. P. Dey, T.K. Nath, Effect of grain size modulation on the magneto- and electronic-transport properties of $La_{0.7}Ca_{0.3}MnO_3$ nanoparticles: the role of spin-polarized tunneling at the enhanced grain surface. Phys. Rev. B **73**, 214425 (2006)
29. A. Dutta, N. Gayathri, R. Ranganathan, Effect of particle size on the magnetic and transport properties of $La_{0.875}Sr_{0.125}MnO_3$. Phys. Rev. B **68**, 054432 (2003)
30. S. Othmani, M. Bejar, E. Dhahri, E.K. Hlil, The effect of the annealing temperature on the structural and magnetic properties of the manganites compounds. J. Alloys Compd. **475**, 46 (2009)
31. R. M'nassri, N. Chniba Boudjada, A. Cheikhrouhou, Impact of sintering temperature on the magnetic and magnetocaloric properties in $Pr_{0.5}Eu_{0.1}Sr_{0.4}MnO_3$ manganites. J. Alloys Compd. **626**, 20 (2015)
32. G. Venkataiah, D.C. Krishna, M. Vithal, S.S. Rao, S.V. Bhat, V. Prasad, S.V. Subramanyam, P. Venugopal Reddy, Effect of sintering temperature on electrical transport properties of $La_{0.67}Ca_{0.33}MnO_3$. Phys. B **357**, 370 (2005)
33. H. Baaziz, N.K. Maaloul, A. Tozri, H. Rahmouni, S. Mizouri, K. Khirouni, E. Dhahri, Effect of sintering temperature and grain size on the electrical transport properties of $La_{0.67}Sr_{0.33}MnO_3$ manganite. Chem. Phys. Lett. **640**, 77 (2015)
34. A. Arroyo, J.M. Alonso, R. Cortés-Gil, J.M. Gonzalez-Calbet, A. Hernando, J.M. Rojo, M. Vallet-Regi, Room-temperature CMR in manganites with 50% Mn^{4+} by generation of cationic vacancies. J. Magn. Magn. Mater. **272**, 1748 (2004)
35. S. Hébert, B. Wang, A. Maignan, C. Martin, R. Retoux, B. Raveau, Vacancies at Mn-site in Mn^{3+} rich manganites: a route to ferromagnetism but not to metallicity. Solid State Commun. **123**, 311 (2002)
36. M. Oumezzine, S. Kallel, O. Peña, N. Kallel, T. Guizouarn, F. Gouttefangeas, M. Oumezzine, Correlation between structural, magnetic and electrical transport properties of barium vacancies in the $La_{0.67}Ba_{0.33-x\square x}MnO_3$ ($x = 0$, 0.05, and 0.1) manganite. J. Alloys. Compd. **582**, 640 (2014)
37. A. Mleiki, R. M'nassri, W. Cheikhrouhou-Koubaa, A. Cheikhrouhou, E.K. Hlil, Structural characterization, magnetic, magnetocaloric properties and critical behavior in lacunar $La_{0.5}Eu_{0.2}Ba_{0.2}\square_{0.1}MnO_3$ nanoparticles. J. Alloys Compd. **727**, 1203 (2017)
38. A.B.J. Kharrat, E.K. Hlil, W. Boujelben, Tuning the magnetic and magnetotransport properties of $Pr_{0.8}Sr_{0.2}MnO_3$ manganites through Bi-doping. Mater. Res. Exp. **5**(12), 126107 (2018)
39. S.V. Trukhanova, I.O. Troyanchuka, N.V. Pushkareva, H. Szymczakb, The influence of oxygen deficiency on the magnetic and electric properties of $La_{0.70}Ba_{0.30}MnO_{3-\delta}$ ($0 \leq \delta \leq 0$ 30) manganite with a perovskite structure. J. Exp. Theor. Phys. **95**, 308 (2002)
40. N.F. Mott, E.A. Davis, *Electronic Processes in Non-crystalline Materials* (Great Britain, Oxford, 1979)
41. A. Ben Hafsia, N. Rammeh, M. Farid, M. Khitouni, Electrical conductivity and dielectric study of $LaBaFe_{0.5}Zn_{0.5}MnO_{6-\delta}$ compound. Ceram. Int. **42**, 3673 (2016)
42. B.P. Jacob, S. Thankachan, S. Xavier, E.M. Mohammed, Dielectric behavior and AC conductivity of Tb^{3+}doped $Ni_{0.4}Zn_{0.6}Fe_2O_4$ nanoparticles. J. Alloys Compd. **541**, 29 (2012)

43. R. Jemaï, R. Lahouli, S. Hcini, H. Rahmouni, K. Khirouni, Investigation of nickel effects on some physical properties of magnesium based ferrite. J. Alloys Compd. **705**, 340 (2017)
44. S.B. Li, C.B. Wang, H.X. Liu, L. Li, Q. Shen, M.Z. Hu, L.M. Zhang, Effect of sintering temperature on structural, magnetic and electrical transport properties of $La_{0.67}Ca_{0.33}MnO_3$ ceramics prepared by Plasma Activated Sintering. Mater. Res. Bull. **99**, 73 (2018)
45. T. Rhimi, M. Toumi, K. Khirouni, S. Guermazi, AC conductivity, electric modulus analysis of $KLi(H_2PO_4)_2$ compound. J. Alloys Compd. **714**, 546 (2017)
46. P.C. Sati, M. Arora, S. Chauhan, M. Kumar, S. Chhoker, Rietveld analysis, magnetic, vibrational and impedance properties of $(Bi_{1-x}Prx)(Fe_{1-x}Zr_x)O_3$. J. Mater. Sci. **24**, 5023 (2013)
47. W. Hzez, A. Benali, H. Rahmouni, E. Dhahri, K. Khirouni, B.F.O. Costa, Effects of oxygen deficiency on the transport and dielectric properties of NdSrNbO. J. Phys. Chem. Solids **117**, 1 (2018)
48. M. Idrees, M. Nadeem, M.M. Hassan, Investigation of conduction and relaxation phenomena in $LaFe_{0.9}Ni_{0.1}O_3$ by impedance spectroscopy. J. Phys. D **43**, 155401 (2010)
49. R. Brahem, H. Rahmouni, N. Farhat, J. Dhahri, K. Khirouni, L.C. Costa, Electrical properties of Sn-doped $Ba_{0.75}Sr_{0.25}Ti_{0.95}O_3$ perovskite. Ceram. Int. **40**, 9355 (2014)
50. S. El Kossi, F.I.H. Rhouma, J. Dhahri, K. Khirouni, Structural and electric properties of $La_{0.7}Sr_{0.25}Na_{0.05}Mn_{0.9}Ti_{0.1}O_3$ ceramics. Physica B **440**, 118 (2014)
51. M. Nadeem, M.J. Akhtar, Melting/collapse of charge orbital ordering and spread of relaxation time with frequency in $La_{0.50}Ca_{0.50}MnO_{3+\delta}$ by impedance spectroscopy. J. Appl. Phys. **104**, 103713 (2008)
52. M. Younas, M. Nadeem, M. Atif, R. Grossinger, Metal-semiconductor transition in $NiFe_2O_4$ nanoparticles due to reverse cationic distribution by impedance spectroscopy. J. Appl. Phys. **109**, 093704 (2010)
53. P.S. Sahoo, A. Panigrahi, S.K. Patri, R.N.P. Choudary, Structural and impedance properties of $Ba_5DyTi_3V7O_{30}$. J. Mater. Sci. **20**, 565 (2009)
54. S. Thakur, R. Rai, I. Bdikin, M. Almeida Valente, Impedance and modulus spectroscopy characterization of Tb modified $Bi_{0.8}A_{0.1}Pb_{0.1}Fe_{0.9}Ti_{0.1}O_3$ ceramics. Mater. Res. **19**, 1 (2016)
55. R. Gaur, K.C. Singh, R. Laishram, Dependence of dielectric properties on sintering conditions of lead free KNN ceramics modified with Li–Sb. World Acad. Sci. Eng. Technol. **9**, 579 (2015)
56. M. Sassi, A. Bettaibi, A. Oueslati, K. Khirouni, M. Gargouri, Electrical conduction mechanism and transport properties of $LiCrP_2O_7$ compound. J. Alloys. Compd. **649**, 642 (2015)
57. S. Zha, C. Xia, G. Meng, Effect of Gd(Sm) doping on properties of ceria electrolyte for solid oxide fuel cells. J. Power Sources **115**, 44 (2003)
58. M.K. Shamim, S. Sharma, S. Sinha, E. Nasreen, Dielectric relaxation and modulus spectroscopy analysis of $(Na_{0.47}K_{0.47}Li_{0.06})NbO_3$ ceramics. J. Adv. Dielectr. **7**, 1750020 (2017)
59. J.H. Joshi, D.K. Kanchan, M.J. Joshi, H.O. Jethva, K.D. Parikh, Dielectric relaxation, complex impedance and modulus spectroscopic studies of mix phase rod like cobalt sulfide nanoparticles. Mater. Res. Bull. **93**, 63 (2017)